Injury Risk Evaluation for Mid-sized Females using Finite Element Human Body Models

Vikas Hasija, Tejas Ruparel, Rohit Kelkar, Matthew J. Craig, Erik G. Takhounts

Abstract Recent studies have shown that females are often at a greater risk of injury than males in frontal crashes. National Automotive Sampling System-Crashworthiness Data System (NASS-CDS) 2000–2015 data analysed in this study showed that 44% of the females involved in frontal crashes were between 25th and 75th height percentile. This study aims to analyse injury risk for mid-sized females in frontal crashes and evaluate how variability within mid-sized females affects the injury risk, and potential countermeasures. Two mid-sized female morphologies of the simplified Global Human Body Models Consortium (GHBMC) model were utilized: a) a simplified 50th percentile adult female GHBMC FE human model (F50); and b) a scaled 50th percentile adult female model (F50-S) obtained by uniformly scaling the simplified GHBMC 5th percentile female model based on seated height. Paired frontal impact simulations were run and the resulting body region injury risks were compared between the models. Statistically significant differences were observed for the head, thorax and lower extremity body regions. Interpretation of machine learning models developed for chest deflection showed the same top four most significant parameters (crash and restraint), but their impact was different for the two models, thus influencing the potential countermeasures for mitigating thoracic injuries.

Keywords Mid-sized females, finite element human body models, injury analysis, machine learning, optimisation.

I. INTRODUCTION

There have been multiple advancements in automotive safety since the late 1980s, and the trends indicate that the total number of injuries has dropped significantly since 1999 [1]. Introduction of new and updated federal motor vehicle safety standards (FMVSS) has led to active and passive safety improvements, which in turn have led to a decline in injuries [2]. Over the years, development of advanced safety systems, such as air bags [3], seat belts with pretensioners and load-limiters [4-5] and modifications in automotive structures, have helped improve occupant protection. Although motor vehicle traffic death rates have increased in recent years, death rates for motor vehicle occupants have decreased by 37% from 1999 through 2019 [6]. The advancement in vehicle safety has led to an overall reduction in injuries and deaths in motor vehicle crashes (MVCs). However, it is important to understand how different occupant demographic segments, based on sex, are affected. Forman *et al.* [7] found that in frontal crashes females are at a higher risk of injury compared to males for both maximum Abbreviated Injury Scale (MAIS) 2+ and 3+ overall and for several body regions. Brumbelow *et al.* [8] also studied frontal crashes and found females to be at significantly higher risk of MAIS2+ injury (odds ratio (OR) of 2.2), even after controlling for vehicle and crash differences, but found a non-significant difference for MAIS3+ injury (OR of 1.45, 95% CI of 0.81 to 2.6). For non-extremity AIS2+ and AIS3+ injuries, they observed smaller differences between females and males overall (AIS2+: OR of 1.31, 95% CI, 0.84–2.04; AIS3+: OR of 0.98, 95% CI, 0.56–1.7). Finally, Brumbelow *et al.* [8] demonstrated that females experienced similar or greater improvements (i.e. reductions in injury risk) with improved vehicle crashworthiness performance (compatible crashes with air bag deployment).

A National Automotive Sampling System-Crashworthiness Data System (NASS-CDS) analysis was conducted to investigate the size (percentile) of female occupants involved in frontal crashes. The analysis was based on weighted NASS-CDS data from 2000 to 2015. Frontal crashes included all passenger cars, light trucks and vans involved in small, moderate or full overlap crashes with principal direction of force (PDOF) ranging from 320° to 40°. Rollover cases were excluded. Cases with belted drivers aged 15+ and MAIS0-6 where an air bag deployed were considered. The data showed that 9% of the females were up to 25th percentile, 44% were between 25th and 75th percentile and 37% were above 75th percentile. This percentile was computed using just the height of the occupants and was based on the National Health and Nutrition Examination Survey (NHANES) 2015–2016

V. Hasija (e-mail: vikas.hasija@dot.gov; tel: +1 (202) 493-0718) is a Mechanical Engineer at National Highway Traffic Safety Administration (NHTSA). T. Ruparel and R. Kelkar are Crash Simulation Engineers at Bowhead (Systems & Technology Group). E.G. Takhounts is a Mechanical Engineer at NHTSA. M.J. Craig is the Chief of Human Injury Research Division at NHTSA.

[9]. For 10% of the cases, height was unknown. As the female population most frequently involved in frontal crashes is close to the 50th percentile female, this study specifically focused on 50th (mid-sized) females.

Variability in anthropometric measures, skeletal geometries and tissue properties, among other differences, may contribute to differences in injury risks for motor vehicle occupants of the same general size, sex and age. Holcombe *et al.* [10], Shi *et al.* [11] and Weaver *et al.* [12] analysed rig cage geometries and observed variability based on age and other factors. Females of the same age belonging to the same percentile may not be the same. Analysing injury risks in a range of frontal impacts, while accounting for variability between occupants, is best accomplished using finite element (FE) human body models (HBMs). HBMs are a powerful tool for evaluating occupant safety as they can represent detailed human anatomical structures. They are omni-directional and can be used for a wide range of loading conditions. In addition, HBMs can be scaled/morphed to generate variations based on size and shape [13], which can be used to study injury trends.

While mid-sized female models have been analysed in rear impacts [14-15], to our knowledge, prior studies have not analysed injury risk for mid-sized females in a range of frontal impacts and have not demonstrated how variability within the same-sized occupant can affect injury risks. The objective of this study was to utilize two mid-sized female morphologies of the simplified Global Human Body Models Consortium (GHBMC) model to evaluate how variability between these models affects injury risk in frontal crashes. To achieve this, paired frontal impact simulations were conducted using the two mid-sized female models in a mid-sized sedan FE model and injury risks were compared across different body regions. For the body regions that showed high relative risk and statistically significant differences, machine learning (ML) models were developed and analyzed to identify the crash and restraint parameters that significantly affect the injury metrics for these high-risk body regions. Subsequently, optimization was carried out using these ML models to inform potential safety countermeasure design considerations.

II. METHODS

Mid-sized female FE models, positioned in the driver compartment of a mid-sized sedan FE model, were used to conduct injury risk analysis. The details on the human models, vehicle model, injury risk analysis and ML models are presented below.

Mid-sized female FE models

Two mid-sized female morphologies of the simplified GHBMC model (Fig. 1) were used in this study: a) a GHBMC 50th percentile female model (F50) [16-17] that was developed by morphing the simplified GHBMC 5th percentile female model (F05) [18-19] to subject anthropometry matching the dimensions of the mid-sized female based on the Anthropometric Survey of US Army Personnel (ANSUR I) dataset [20]; and b) a scaled 50th percentile female model (F50-S) obtained by uniformly scaling the F05 model based on seated height. The F50-S model was generated by scaling up the F05 model by a factor of 1.103, which is the seated height ratio between a 50th female [21] and the F05 model. Additional details about the F50-S and F50 models are provided in Appendix A (Table A1). The F50 model weighs 62 kgs, while the F50-S model weighs 69 kgs. However, according to the GAO report [22], the average weight of a 50th percentile US female is 73 kgs, making the F50-S model closer in weight to the average US female. While the F50-S model is not based on measured data like the F50 model, it is directly scaled from the F05 model, which is the only female model developed based on actual scans of a female. Furthermore, when compared with 50th percentile female data from the ANSUR-II anthropometry database [23] (Appendix A, Table A1), the F50-S model is found to be closer than the F50 model in terms of total mass, seated height, chest depth, waist breadth, waist depth, and hip breadth. Therefore, the F50-S model may represent a realistic mid-sized female body. Currently, there is no unique definition of mid-sized females. While the F50 and F50-S models are different in terms of development methodology, they both may represent mid-sized females.

The F50 model has been validated by GHBMC but no validation was carried out for the F50-S model. However, since the F50-S model is a scaled version of the fully validated F05 model, it is assumed that the F50-S model possesses a certain degree of validation. In addition, there is currently no validation data specific for 50th percentile females. Instead, the validation corridors for 50th percentile females are developed by scaling 50th percentile male corridors. Without further PMHS tests, it is challenging to determine a reasonable response for 50th percentile females. In the absence of such information, it is difficult to determine which model response is correct if validation results for the F50 and F50-S models are different. Thus, validation of these models will be a

focus of future research as more data becomes available for 50th percentile female responses.

Simplified GHBMC models run in under two hours for a 150 ms crash event on 56 processors compared to over 20 hours for detailed GHBMC models. Since a significant number of simulations (200 per model) were run, simplified models were chosen for computational efficiency.

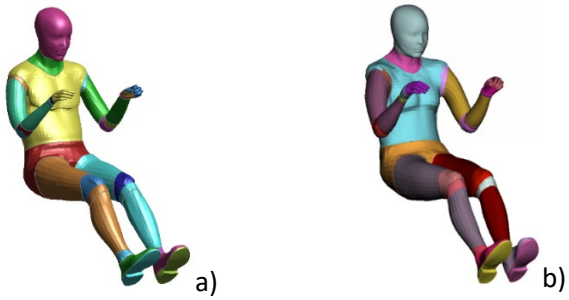

a) b)

Fig. 1. a) F50 and b) F50-S mid-sized female models.

Vehicle model

A validated 2014 Honda Accord FE model [24] (Fig. 2a) with 3.1 million elements was selected for this study. For simulating multiple frontal impact scenarios within a feasible timeframe, a simplified driver compartment (Fig. 2b) was generated by extracting the required components from the Honda Accord FE model. This simplified driver compartment had frontal and side curtain air bags, steering wheel and column, dash and knee bolster, side door, roof rails, A-pillar, B-pillar, seat, floor, and seat belt with retractor, pretensioner and load limiter. In this study, the side door, roof rails, B-pillar, dash and floor were made rigid. The A-pillar and knee bolster were kept deformable. Additionally, a collapsible steering column was modeled and utilised in this study. This simplified driver compartment only had 485,000 elements, which helped reduce simulation runtime.

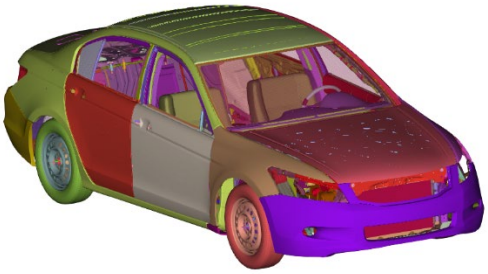

Fig. 2a. Honda Accord vehicle FE model.

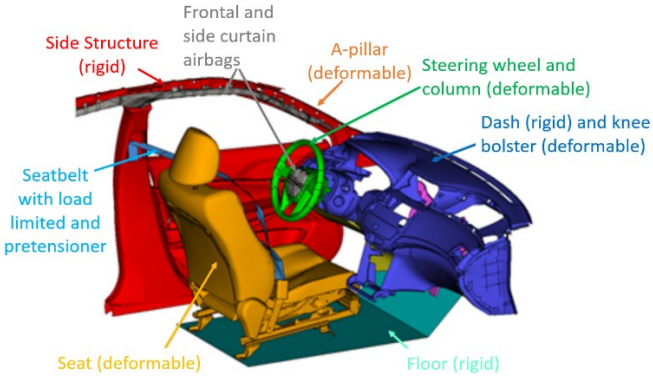

Fig. 2b. Simplified driver compartment.

Occupant positioning

Since there is no procedure for positioning the 50th percentile female, positioning of these models was done in reference to the 50th percentile male model. The simplified GHBMC 50th percentile male model (M50) [25-26] was first positioned in the simplified driver compartment based on a physical test. NHTSA test number 8035 (Hybrid-III 50th percentile male anthropomorphic test device (ATD) in the driver seat of a 2013 Honda Accord, https://www-nrd.nhtsa.dot.gov/database/veh/) was selected. The positioning for the M50 model was based on the physical test clearance measurements (Appendix B, Fig. B1). The F50-S model was first positioned in a similar seat track position as the M50 model. In this position, the feet of the F50-S model were not in contact with the toepan. The seat was then moved forward on the seat track such that the feet were contacting the toe pan and the hands were on the steering wheel. This procedure resulted in the F50-S model seat track position being 44 mm forward of the M50 model seat track position (Appendix B, Fig. B2). The F50 model was positioned in a similar seat track position as the F50-S model, which resulted in the F50 model H-point being lower than the F50-S model H-point by 8 mm. The extremities were articulated so that the feet of the F50 model were in contact with the toepan and the hands were on the steering wheel. In this position, because of different seating postures and anthropometries (e.g. smaller femur length for the F50 model compared to the F50-S model; 370 mm versus 393 mm, respectively), the knee-to-dash distance for the F50 model was different from that for the F50-S model. The knee bolster position was adjusted fore-aft (moved towards the occupant by 58 mm) such that the knee-to-dash

distance was similar to the F50-S model. Appendix B (Fig. B3) shows the F50 and F50-S models in their baseline seating position. The knee-to-dash distance was not fixed but was varied in this study, as described below in section *Paired simulations and injury risk comparison*. The baseline knee-to-dash distance was kept the same for the two models so that this distance could be varied by the same amount around the baseline.

Crash pulse

The crash pulse from NHTSA test number 9476 (frontal-oblique impact for 2015 Chevrolet Malibu, impacted by Oblique Moving Deformable Barrier (OMDB) with 35% overlap, https://www-nrd.nhtsa.dot.gov/database/veh/) was used as the baseline (Appendix C, Fig. C1). The crash pulse for a given vehicle can vary depending on factors such as the type and stiffness of impacting surface, the degree of frontal overlap, and principal direction of force (PDOF). Additionally, different vehicles of the same size (e.g., mid-sized sedans) may exhibit different crash pulses under the same conditions. To keep the number of variables manageable in this study, crash pulse shape was kept constant and only the crash pulse magnitude was scaled to achieve different Delta-Vs.

Injury risk functions and scaling factors

The injury risk functions developed for the M50 (Table I, column 2) were used to compute the probability of AIS2+ injury. For each model (F50 and F50-S), the injury metrics (Table I) were computed for all simulations, followed by the computation of an average value for each injury metric across all simulations. The average injury metric values were scaled to obtain the corresponding M50 injury metric value and then used in the risk functions to obtain the probability of AIS2+ injury for these models. Table I lists the scaling factors used for the F50-S and F50 models with respect to M50. Injury assessment reference values (IARVs) were used to compute the scaling factors between 50th male and 50th female. While the IARVs for 50th (mid-sized) male and 5th (small) female are available [27], there are currently no established IARVs for 50th females. In the absence of such data, a study was conducted to evaluate the chest deflection IARV for 50th females (see last paragraph under *Results: Paired simulations and Injury risk comparison*). This study demonstrated that 5th female IARVs may be used for 50th females. Thus, the scaling factors between 50th male and 50th female were computed based on the 50th male and 5th female IARVs. The scaling factor used for chest deflection was 1.212, which is the ratio of chest deflection IARV for mid-sized male and small female, respectively [27]. Similarly, the scaling factor for femur forces was 1.471, which is the ratio of femur load IARV for mid-sized male and small female, respectively [27]. The scaling factor of 1.389 used for upper and lower tibia forces was taken from Kuppa *et al*. [28].

TABLE I

INJURY METRICS, RISK FUNCTIONS AND SCALING FACTORS

Injury metric (name used in figures)	AIS2+ risk functions (M50)	Scaling factors M50/F50(-S)
BrIC (BrIC)	$1-e^{-\left(\frac{BrIC-0.523}{0.324}\right)^{1.8}}$ [29]	1.0
HIC_{15} (HIC15)	$\Phi\left[\frac{\ln HIC_{15}-6.96362}{0.84687}\right]$ [27]	1.0
N_{ij} (Nij)	$\frac{1}{1+e^{(5.819-5.681Nij)}}$ [30]	1.0
Chest deflection (CD)	$\frac{1}{1+e^{(1.8706-0.04439\mathrm{Dmax})}}$ [27]	1.212
Femur forces (Femur)	$\frac{1}{1+e^{(5.795-0.5196\,F)}}$ [27]	1.471
Upper tibia forces (TibiaU)	$\frac{1}{1+e^{(5.7415-0.8189F)}}$ [30]	1.389
Lower tibia forces (TibiaL)	$\frac{1}{1+e^{(3.7544-0.4683F)}}$ [30]	1.389

Regarding N_{ij}, the critical intercept values for the 50th male (Appendix D, Table D1) were taken from Craig *et al.* [30]. To obtain the critical intercept values for the 5th female, the 50th male tension and compression intercept values were scaled by 0.75, and the flexion and extension intercept values were scaled by 0.5. The scaling factors are based on Eppinger *et al.* [27]. These 5th female critical intercept values (Appendix D, Table D1) were utilised for the F50-S and F50 models. Chest deflection was computed as the maximum of the absolute peak fore-aft or

anatomical x-axis deflection of several sternum nodes. Femur forces were computed as the absolute maximum of the axial force in the load cells located at the left and right mid-femur. Upper tibia forces were computed as the absolute maximum of the axial force in the load cells located at the left and right upper tibia, and lower tibia forces were computed as the absolute maximum of the axial force in the load cells located at the left and right lower tibia.

Paired simulations and injury risk comparison

To compare injury risks, paired simulations were run with the two human models. The points for the paired simulations were generated using space filling sampling scheme in LS-OPT [31] by varying both the crash and restraint related parameters (Appendix E, Table E1). A total of 200 points were generated and simulations were run with these points for each human model for a total of 400 simulations.

NASS-CDS field data analysis performed by Takhounts *et al.* [32] showed that more than 99% of all frontal impacts were between PDOF values of -30° and +30°. Hence, for this study PDOF was varied from -30° (near side) to 30° (far side). A baseline value of 1.0 used for the frontal and side curtain air bag mass flow rate refers to using the validated mass flow rate curve, which is then scaled by ±25%. The side curtain air bag was set to fire at the same time as the frontal air bag. The range (5–45 ms) for air bag firing times was selected by analysing Event Data Recorder (EDR) data from several Crash Injury Research and Engineering Network (CIREN) cases. The collapsible steering column modeled in this study had a baseline column collapsing force of 3000 N. This baseline force of 3000 N was obtained by evaluating data from a quasi-static physical test conducted by NHTSA and was also targeted to be large enough that the column would not collapse from the force applied by the air bag on the steering wheel during deployment. At 3000 N, the column withstands the air bag deployment force and at a maximum value of 12000 N the column is locked. For the seat belt load limiter and pretensioner, baseline values of 3000N and 1000N were used respectively. These were based on analyzing the NHTSA crash test data. The seat belt load limiter was varied between 1000 N and 5000 N, whereas the seat belt pretensioner was varied between 1000 N and 3000 N. These parameters were varied over a wider range compared to those typically used in current real-world restraint systems. Given the range for the load limiter and pretensioner, there could be cases where the pretensioner value is higher than the load limiter value. To ensure that the pretensioner value is always less than or equal to the load limiter value, a constraint was added to represent this condition. The friction coefficient between the shoe and the floor was varied from 0.001 to 0.5, whereas the friction coefficient between the head and frontal/side curtain air bags was varied from 0.001 to 1.0. A numerical friction coefficient of 1.0 in Dyna does not necessarily represent a sticky contact. In order to create a truly sticky contact, a much higher numerical friction coefficient (> 2.0) is required in Dyna. However, such high values may not be representative of real-world scenarios and were therefore not considered in our analysis. Instead, the numerical friction coefficient was varied up to a maximum value of 1.0 (non-sticky). In this study, knee-to-dash distance was also varied. This was varied by moving the dash and the knee bolster and not the seat, so that the simulations could be performed with a single model set-up. A value of 1.0 for the knee-to-dash distance represents the baseline set-up distance. This distance was then varied by ± 25%.

Forman *et al.* [7] showed high injury risk for the brain and thorax body regions relative to other body regions. Of these two high-injury-risk body regions, the thorax body region was further analysed between the two human models (F50 and F50-S) with respect to material properties and thoracic skeletal geometry. Material properties and thicknesses of the skeletal thorax were compared between the F50 and F50-S models. For geometrical comparison, rib and sternum angles along with the chest depth were compared. The measurement techniques are shown in Fig. 3. Rib angles were computed by measuring the angle between the dashed line (defined using the posterior aspect of ribs 4 and 7) and the angled red lines determined by the posterior and anterior articulations of the ribs (Fig. 3a). Sternum angle was computed by measuring the angle between the dashed line (defined using the posterior aspect of ribs 4 and 7) and the angled red line (defined from the inferior-most anterior point to the superior-most anterior point on the sternum) (Fig. 3b). Two chest depth measurements were made: 1) using a bounding box (dashed lines) around the seated occupant ribcage (Fig. 3c); and 2) between the mid sternum and a point posteriorly horizontal to it on the thoracic spine (red line, Fig. 3c).

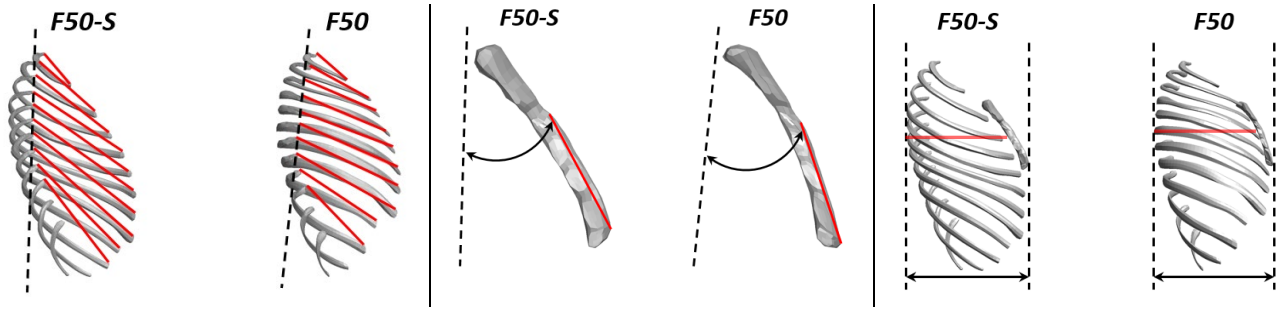

Fig. 3. A. Rib angles, b. sternum angle, and c. chest depth measurement techniques.

Machine learning models and optimisation

Using the data from the paired simulations, ML models were developed to predict injury metrics (BrIC and chest deflection) for the brain and thorax body regions. Although injury metrics were computed for other body regions, ML models were only developed for the brain and thorax body regions as they show higher risk relative to other body regions [7]. A total of four ML models were trained, one for each injury metric (BrIC and chest deflection) for the two human models. This was done to understand the important crash and restraint related parameters that influence these injury metrics for each human model. Simple linear regression [33], linear regression with L1/L2 regularisation (Lasso/Ridge) [34-35], support vector regressor (SVR) [36], and ensemble methods, namely random forest regressor [37] and XGBoost regressor [38], were used to develop the ML models using K-fold cross-validation [39]. In this study, K=10 was used. Of all the ML methods used to develop the predictive model, the one that gave the best score on the validation set (best generalisation) was selected. The trained (cross-validated) ML models corresponding to the selected method were further evaluated on a separate, previously unseen (test) dataset. For this purpose, thirty additional paired FE simulations (distinct from the 200 simulations) were performed, and correlation coefficients were computed between the predicted outputs of the ML models and the actual FE outputs to assess the quality of the trained ML models.

Developing a ML model using a supervised learning approach requires both inputs and the corresponding outputs. Crash and restraint related parameters were used as inputs and the corresponding injury metric was used as the output. PDOF, which was a discrete parameter when running FE simulations, was converted to a continuous scale (0–360^0). The input data were normalised using standard scaling (Eq. 1) before training the ML models:

$$z = \frac{x-\mu}{\sigma} \qquad (1)$$

where x is the unnormalised value, μ is the mean, σ is the standard deviation and z is the normalised value.

Scikit-learn [40] Python library was used for training the ML models. Once the ML models were trained, Shapley values [41] were used to interpret the models. SHAP [42] Python library was used for this purpose and parameters that significantly affect the injury metrics (BrIC and chest deflection) were identified for each human model. Optimisation was also performed using the trained ML models to find a single set of restraint parameters that would reduce the injury metrics (BrIC and chest deflection) below their respective IARVs for the two human models at NCAP Delta-V of 35 mph across a range of PDOFs. Three different frontal crash PDOFs were considered: 0^o, 20^o and 340^o. For BrIC, IARVs of 0.8 and 1.0 (50% risk of AIS2+ and AIS4+ brain injury, respectively) were used. For chest deflection, IARV of 52 mm (33% risk of AIS3+ thoracic injury) was used. Optimisation was set up using scikit-optimize [43] and the optimal points (restraint parameters) from the optimisation runs were evaluated using the trained ML models predictions. Gradient boosted trees based sequential optimisation algorithm available in sckit-optimize was used. Appendix F (Table F1) shows the restraint parameters that were varied for optimisation.

III. RESULTS

Paired simulations and Injury risk comparison

Of the 200 paired simulations between F50 and F50-S, 149 pairs of simulations terminated normally. These were used for the analysis. The Delta-V and PDOF distributions for these 149 points are shown in Appendix G (Fig. G1). From these 149 paired simulations, the average value for the various injury metrics (Table I) was calculated for each human model. Using these average injury metric values, the injury risks were computed and compared

between the two models (Fig. 4). Independent samples t-test was also conducted for each injury metric between the two models and the corresponding *p* values are shown in Fig. 4 as well.

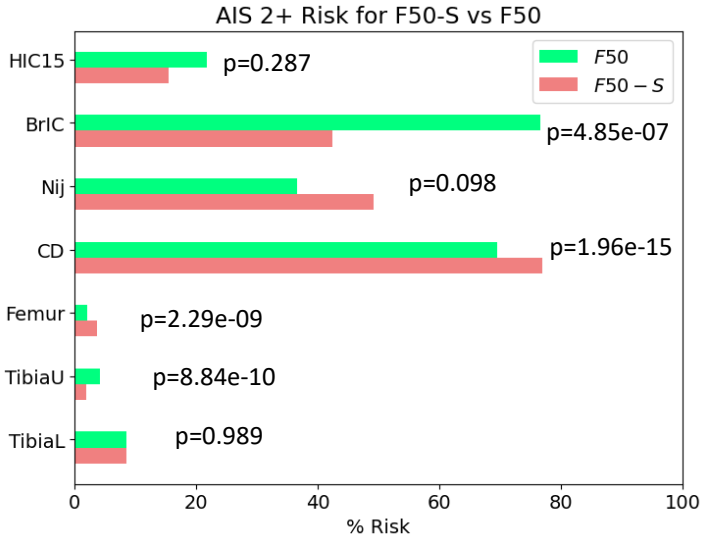

Fig. 4. Injury risk comparison across body regions between F50 and F50-S.

It can be observed from Fig. 4 that there are statistically significant differences between the two models with respect to the brain, thorax and lower extremity body regions. Of these, the brain and thorax body regions show higher injury risk than the lower extremity body region for both models.

The F50 model demonstrated higher head/brain injury risk and lower thoracic injury risk compared to the F50-S model. Material properties and geometry of the skeletal thorax were analysed to understand the reason for the differences in chest deflections between the two models. It was found that the material properties and thicknesses of the skeletal thorax were the same for both the models, but there were differences in the skeletal geometry. Table II shows the rib angles, sternum angle and chest depth for the F50-S and F50 models. Average rib angle (ribs 4–8) was higher for the F50 model, whereas the sternum angle was higher for the F50-S model. The chest depth for the F50 model was slightly higher than the F50-S model. These differences in the thoracic skeletal geometry may be the main reason for differences observed in chest deflections between the two mid-sized female models (F50 and F50-S).

TABLE II

RIB ANGLES, STERNUM ANGLE, AND CHEST DEPTH FOR THE F50-S AND F50 MODELS

Rib #	Rib Angles (degrees)		Sternum Angle (degrees)		Chest Depth (mm)	
	F50-S	F50	F50-S	F50	F50-S	F50
1	35.59	45.01	28.94	22.83	182.78 (Bounding box) 116 (Mid-sternum)	186.30 (Bounding box) 121 (Mid-sternum)
2	45.64	60.42				
3	49.50	62.58				
4	53.30	64.64				
5	53.01	63.46				
6	51.94	61.9				
7	48.19	57.64				
8	45.00	52.88				
9	39.08	44.51				
10	32.53	36.7				
11	---	---				
12	---	---				
Average Rib Angle of 4–8	50.28	60.10				

The F50 and F50-S models were also compared in terms of the number of cases with AIS1 (one fractured rib), AIS2 (two fractured ribs) and AIS3 (3+ fractured ribs) thoracic skeletal injuries. Rib fracture was based on plastic

strain threshold of 0.018 for the cortical bone [44]. The results are presented in Fig. 5. It can be observed that the F50-S model had a higher number of cases for all three AIS levels compared to the F50 model. Of the 149 simulations, 72 had at least one rib fracture for the F50-S model compared to 33 for the F50 model.

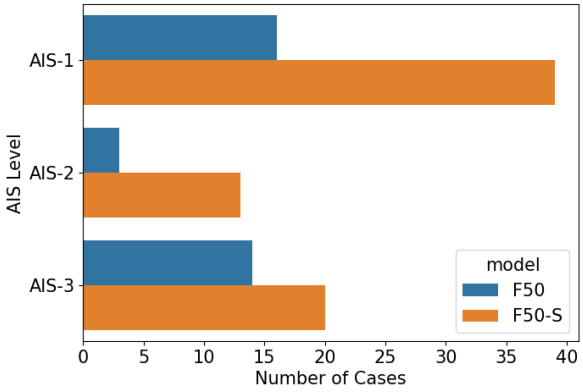

Fig. 5. Number of cases with thoracic skeletal injuries at different AIS levels for the F50 and F50-S models.

To evaluate the chest deflection IARV for 50th females, regression plots were generated between peak chest deflection and maximum rib plastic strain for the two models using the paired simulation data (Fig. 6). Maximum rib plastic strain represents the maximum plastic strain across all ribs (left and right). Each plot in Fig. 6 shows a regression line in blue, a vertical red line representing the IARV value of 52 mm for 5th (small) female, and a horizontal red line representing the plastic strain threshold (cortical bone failure) value of 0.018. The regression lines for the F50-S and F50 models intersect the plastic strain threshold line at 52 mm and 55 mm, respectively, which is similar/close to the chest deflection IARV for the 5th female. If chest depth (similar to Eppinger *et al.* [27]) is used to compute the chest deflection IARV for 50th females, the value is 61.1 mm (product of the chest deflection IARV for 50th male (63 mm) and the ratio of 50th female chest depth (24.5 cm) to 50th male chest depth (25.3 cm) [23]). Since the F50 and F50-S model results (Fig. 6) were closer to the 5th female IARV and given that there is no unique definition of a 50th female, 5th female IARVs were used for the 50th females in this study.

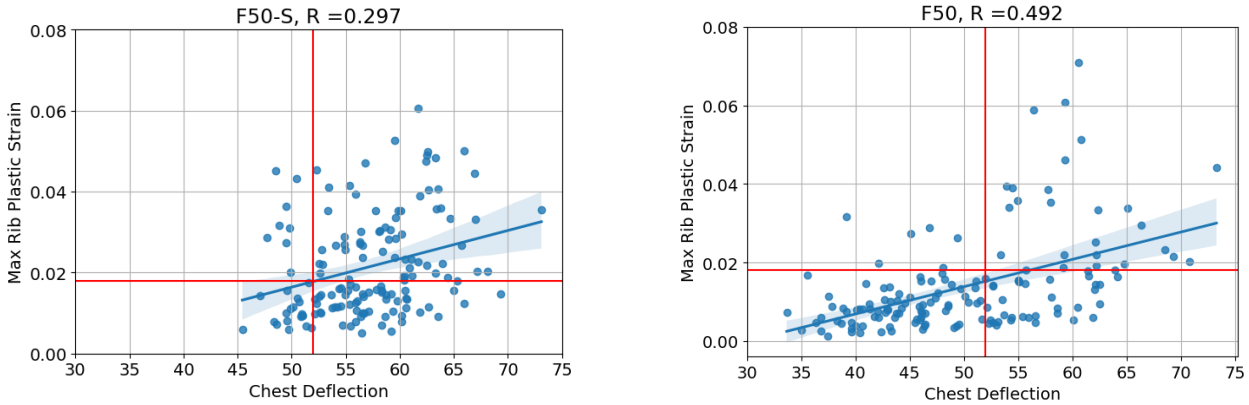

Fig. 6. Chest deflection vs maximum rib plastic strain for the F50-S and F50 models

Machine learning models and Optimisation

Of the algorithms used in this study for building ML models, XGBoost had the best validation score for both injury metrics (BrIC and chest deflection) for both human models (Appendix H, Table H1) and was therefore chosen. These XGBoost models were further evaluated on an unseen (test) dataset and the corresponding test scores are presented in Appendix H (Table H1) as well. The models achieved good performance on the test dataset, with all scores exceeding 0.75. The trained XGBoost models were interpreted using the SHAP library. The results of interpretation are presented in the form of a bar chart (Fig. 7), which shows the average impact of different parameters on the injury metric and is organised by importance, with the most significant parameters on top.

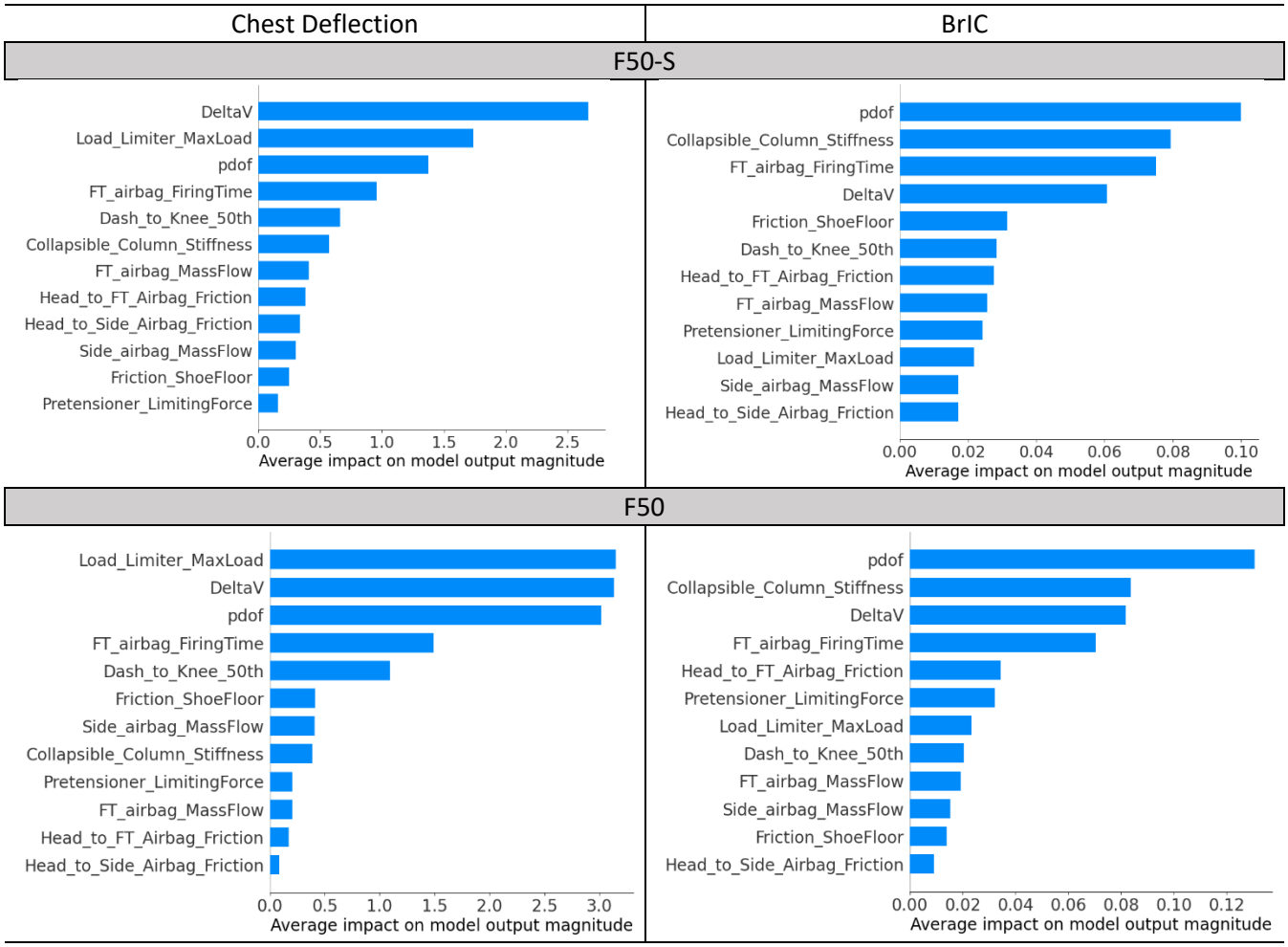

Fig. 7. Impact of different parameters on chest deflection and BrIC for F50-S and F50 models.

Violin plots that show the correlation of each of these parameters with the injury metric are presented in Appendix I (Fig. I1). In the violin plots, when moving from left to right, a colour variation blue-maroon-red signifies positive correlation and vice-versa. The parameters are organised by importance and SHAP values can range from negative to positive in the violin plots. A negative SHAP value at low feature (parameter) value suggests that low values of the feature push the prediction value (injury metric) down and a positive SHAP value at high feature value suggests that high values of the feature push the prediction value (injury metric) up. It can be observed from Fig. 7 and violin plots (Appendix I, Fig. I1) that for both the F50 and F50-S models, the top five parameters affecting chest deflection are the same, namely Delta-V, load limiter, PDOF, frontal air bag firing time and knee-to-dash distance. However, for the F50-S model, Delta-V is the most important parameter followed by the load limiter, whereas for the F50 model, load limiter and Delta-V are equally important. For both models, chest deflection has a positive correlation with Delta-V, frontal air bag firing time, knee-to-dash distance and load limiter, and a negative correlation with PDOF. With respect to BrIC, it can be observed that both the models share the same top four parameters, namely PDOF, Delta-V, frontal air bag firing time and collapsible steering column force, with PDOF being the most important parameter. BrIC shows a positive correlation with these four parameters for both the models.

Predicted values (using the trained XGBoost models) of chest deflection and BrIC for the two mid-sized female models based on the baseline value of restraint parameters (Appendix E, Table E1) are presented in Fig. 8. Chest deflection and BrIC values are shown for three different PDOFs (0°, 20°, 340°) at Delta-V of 35 mph. The dashed horizontal dark blue line in the chest deflection plot represents the IARV value of 52 mm. The dashed horizontal red lines at 0.8 and 1.0 in the BrIC plot represent 50% risk of AIS2+ and AIS4+ brain injury, respectively. It can be observed that while the BrIC values are below 0.8 for both the human models, chest deflections are higher than the IARV of 52 mm for the F50-S model for all three PDOFs, and for PDOF of 0° and 340° with the F50 model.

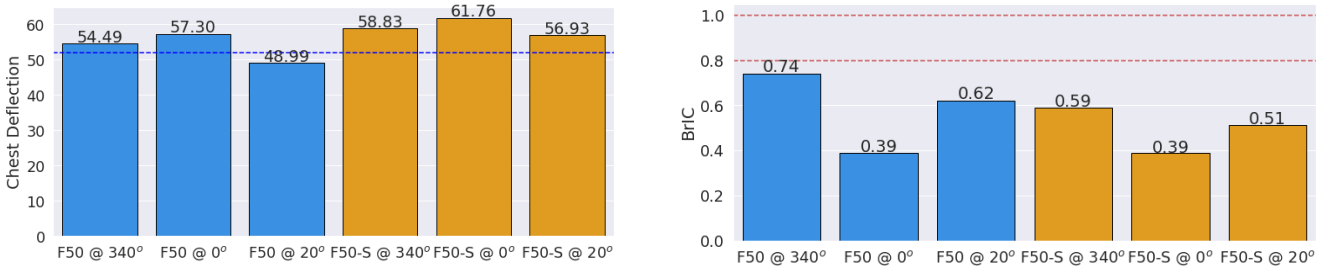

Fig. 8. ML models' predictions with baseline restraint parameters.

As the chest deflections are higher for the F50-S model compared to the F50 model for all three PDOFs (Fig. 8), a single objective optimisation was carried out wherein the chest deflection for the F50-S model was minimised. This optimisation was conducted at Delta-V of 35 mph for a single PDOF of 0° (PDOF with highest chest deflection). Table III shows the optimal point obtained from the single objective optimisation. Both the F50 and F50-S models were evaluated using this optimal point for a range of PDOFs at Delta-V of 35 mph (Fig. 9).

TABLE III
RESTRAINT PARAMETERS WITH SINGLE OBJECTIVE OPTIMISATION AT 35 MPH

Restraint Parameters	Optimal Point
Frontal air bag mass flow rate	0.86
Steering column collapse force	4482 N
Load limiter	1237 N
Pretensioner	1095 N
Frontal and side curtain air bag firing time	7.8 ms
Side curtain air bag mass flow rate	0.79
Head-frontal air bag friction coefficient	0.04
Head-side curtain air bag friction coefficient	0.32

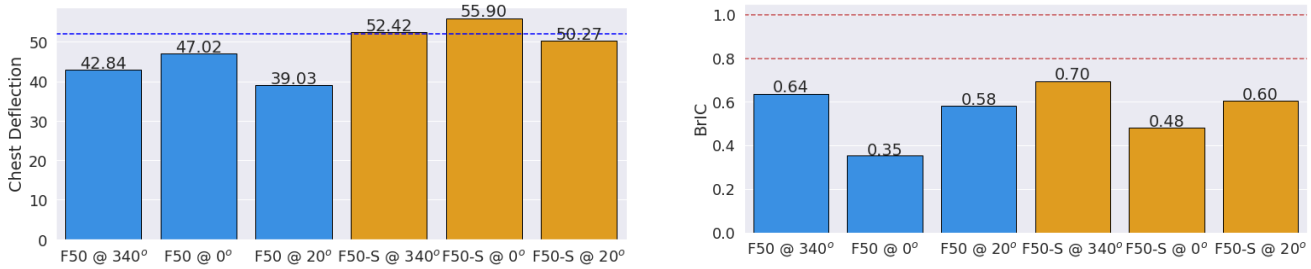

Fig. 9. BrIC and chest deflection values with optimal point from single objective optimisation.

It can be observed from Fig. 9 that with the optimal point (Table III), the chest deflections for the F50 model dropped below the IARV of 52 mm for all three PDOFs. Even for the F50-S model, the chest deflections reduced but were still above the IARV of 52mm for PDOF of 0° and 340°. With the optimal point, BrIC values reduced slightly for the F50 model, but they increased for the F50-S model compared to the corresponding values with the baseline parameters (Fig. 8).

It is evident from the results of single objective optimisation that just controlling the restraint parameters simulated in this study does not help reduce the chest deflections for the F50-S model below the IARV of 52 mm. Figure 7 shows that the chest deflection for the F50-S model is most greatly affected by Delta-V. Thus, single objective optimisation was carried out at Delta-V of 25 mph instead of 35 mph at PDOF of 0° to evaluate chest deflection for the F50-S model. The optimal point and the results for both the human models evaluated using this optimal point are shown in Table IV and Fig. 10, respectively. It can be observed from Fig. 10 that at Delta-V of 25 mph, the chest deflection for the F50-S model reduced below the IARV of 52 mm for all three PDOFs, but again this is achieved with a lower load limiter value of 1751 N. If the load limiter value is fixed at 3000 N (baseline) and single objective optimisation is performed at Delta-V of 25 mph and PDOF of 0°, the chest deflection for the F50-S model at PDOF of 0° slightly exceeds the IARV of 52 mm (52.49 mm, Fig. 11). For the F50 model, the chest

deflections are below the IARV. BrIC values for both the models are below the IARV as well. The optimal point corresponding to this optimisation is also shown in Table IV.

TABLE IV
RESTRAINT PARAMETERS WITH SINGLE OBJECTIVE OPTIMISATION AT 25 MPH

Restraint Parameters	Optimal Point	Optimal Point with Fixed Load Limiter (3000 N)
Frontal air bag mass flow rate	0.84	0.76
Steering column collapse force	3188 N	3421N
Load limiter	1751 N	3000 N
Pretensioner	1751 N	2137 N
Frontal and side curtain air bag firing time	7.2 ms	7.1 ms
Side curtain air bag mass flow rate	1.206	1.16
Head-frontal air bag friction coefficient	0.0095	0.686
Head-side curtain air bag friction coefficient	0.48	0.293

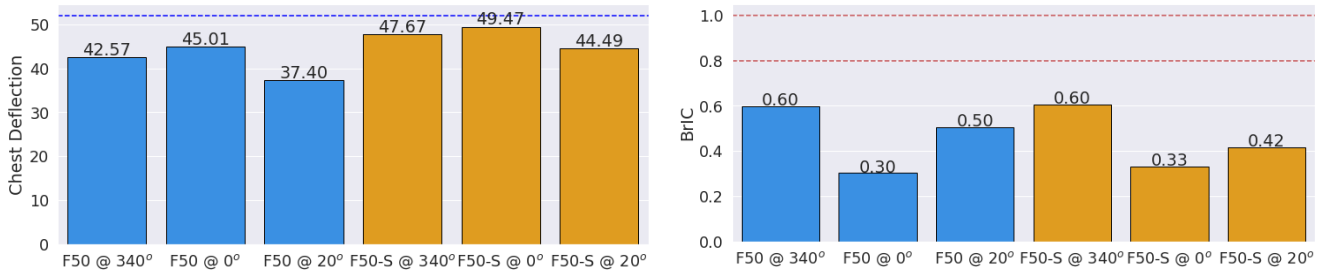

Fig. 10. BrIC and chest deflection values with optimal point from single objective optimisation at Delta-V of 25 mph.

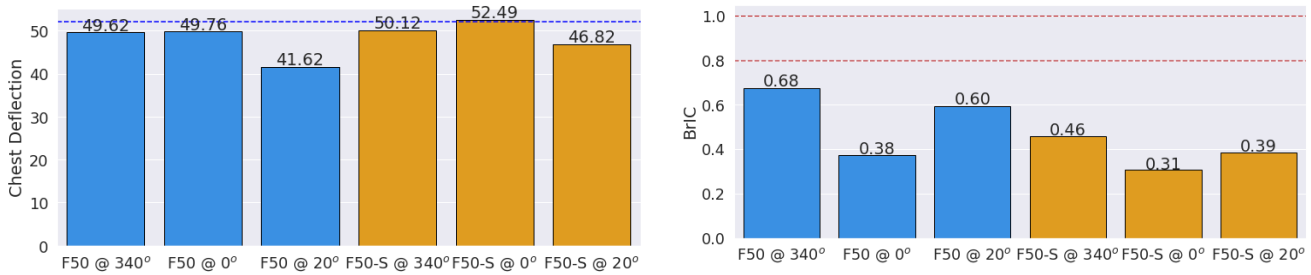

Fig. 11. BrIC and chest deflection values with optimal point from single objective optimisation at Delta-V of 25 mph with load limiter fixed at 3000 N.

IV. DISCUSSION

In this study, injury risk analysis was conducted for mid-sized females in frontal crashes using finite element human body models. In addition to the GHBMC 50th percentile female model, a 50th percentile female model scaled from the GHBMC 5th percentile female model was also used. Such scaled 50th female models have been used in other studies as well. Sato *et al.* [15] generated a scaled FE model of an average size female by scaling the Total Human Model for Safety (THUMS) 5th percentile female model [45] to investigate effects of spinal alignment patterns on cervical vertebral motion in rear-end impacts. Carlsson *et al.* [14] also used scaling (mass and length) to generate the EvaRID (50th percentile female) model from the BioRID II (50th percentile male) FE model to evaluate whiplash injury risk in rear impacts. For our study, the GHBMC family of models were used to avoid any variability due to model construction affecting the outcome.

The F50 and F50-S models were compared with other open source 50th percentile female HBMs i.e., THUMS [46] and VIVA [47], as well as with 50th percentile female data from the ANSUR-II anthropometry database to evaluate variability among mid-sized female HBMs. The results, presented in Appendix A (Table A1),

reveal that there is variability in the majority of measurements among the HBMs. The F50-S model is closest to the ANSUR-II data in terms of total mass and seated height, compared with other HBMs. Additionally, the F50-S model has the longest femur length, while the F50 model has the longest tibia length. None of the HBMs match all of the measurements from the ANSUR-II dataset, however, the F50-S model demonstrates greater similarity to the ANSUR-II data than the other models.

The knee-to-dash distance in this study was varied independently because: a) due to lack of a seating protocol for 50th females, the F50 and F50-S models were positioned in reference to the M50 model, which itself was positioned based on a Hybrid-III 50th percentile male ATD test. However, due to differences between human models and ATDs, the resulting knee-to-dash distance for the M50 model was not exactly the same as that of the Hybrid-III 50th male ATD. Moreover, if the M50 model was positioned based on a Test Device for Human Occupant Restraint (THOR) 50th percentile male ATD test, the resulting knee-to-dash distance would have been different (longer femur for the THOR compared to Hybrid-III; 396 mm versus 376 mm, respectively), affecting the F50 and F50-S models as well; b) the knee-to-dash distance may differ for the same occupant when seated in different vehicles due to variability across the fleet. Further investigation is necessary to determine whether this variability in knee-to-dash distance across the fleet correlates with the body-to-air bag distance. Without this data, the knee-to-dash distance was independently adjusted to simulate various vehicles; and c) currently, there is no research on how the anthropometric variability affects seating preferences. For example, the same sized individuals (e.g., 50th female) could have different femur lengths while having the same height. The different femur lengths may result in different knee-to-dash distances. However, it remains unclear whether an individual would adjust the distance to the steering wheel proportional to their femur length or knee-to-dash distance. Further research is necessary to investigate this relationship. In this study, knee-to-dash and chest-to-steering wheel distances were assumed to be independent determined by individual anthropometry and seating preferences. Including the chest-to-steering wheel distance as an independent parameter in the study would have substantially increased the number of runs per model (by three-fold assuming only 3 steering wheel positions). In addition, steering wheel angle is also adjustable. Assuming only 3 angle values, inclusion of these two additional parameters (steering wheel position and angle) would have increased the number of runs at least 6-fold per model making the study almost unfeasible. Because of these reasons, the knee-to-dash distance was not fixed but rather varied as an independent variable to study the effect of this parameter on injury metrics.

Paired frontal impact simulations were run to evaluate injury risks for the two mid-sized female models. Even with very similar seating positions (Appendix B, Fig. B3), statistically significant differences were observed with regard to BrIC, chest deflections, femur forces, and upper tibia forces (Fig. 4). For both mid-sized female models, the brain and thorax body regions showed high injury risks; generally, more than 50% (Fig. 4). This observation is in agreement with Forman *et al.* [7] where, for model year 2009+, the authors showed the highest AIS2+ injury risk for concussion and thoracic skeletal injuries. Even though there were statistically significant differences between the two models for femur and upper tibia forces, the corresponding injury risks, at less than 10%, were much lower than observed for the brain, neck and thorax (Fig. 4).

Brain injury risk was higher for the F50 model compared to the F50-S model (Fig. 4). This may be due to differences in the head mass, moment of inertias (Appendix A, Table A1), and initial position of the head (F50 head is slightly forward compared to F50-S, Appendix B, Fig. B3). The two models were not adjusted to have similar initial head positions, head mass or moment of inertias since this kind of variability is expected within the same population size. Thoracic injury risk, on the other hand, was higher for the F50-S model compared to the F50 model (Fig. 4). In addition to higher chest deflections, rib fracture analysis showed a greater percentage of rib fractures (118%) for the F50-S model compared to the F50 model. Since the rib cage material properties and torso mass (Appendix A, Table A1) were similar between the two models, different thoracic skeletal geometries (higher sternum angle and smaller rib angles for the F50-S model compared to the F50 model, Table II) may be the reason for differences in chest deflections and number of rib fractures between the two models.

Regarding neck injuries, the two models did show differences in N_{ij} values, but these were not statistically significant. Despite similar neck construction for the F50 and F50-S models, variations in the Nij values between the two can be attributed to differences in both the head inertial properties and neck anthropometry (smaller neck column length for the F50-S model compared to the F50 model; 112 mm versus 125 mm, respectively). These differences may result in different forces and moments for the same crash and restraint system parameters. The neck injury risk was relatively high for both models, ranging from 35% to 50% (Fig. 4). For the

F50-S model, it was even slightly higher than the corresponding brain injury risk (Fig. 4). Forman *et al.* [7], in general, documented much lower risk for neck injuries when compared with brain, thoracic and lower extremity injuries. The reason for high neck injury risk in this study may be due to the critical intercepts used for N_{ij} computation. Critical intercepts for the 5th female (Appendix D, Table D1) were used for the mid-sized female models. Further research is needed to help establish these critical intercepts for the mid-sized females.

To reduce brain and thoracic injuries, it is important to understand the parameters that affect BrIC and chest deflection. Machine learning models developed for each human model provided such insight. Crash parameters (Delta-V and PDOF) affected both BrIC and chest deflection and were among the top four parameters for both injury metrics for both models (Fig. 7). Of the tunable restraint parameters, air bag firing time and load limiter were important for chest deflection (Fig. 7) and showed a positive correlation with it (Appendix I, Fig. I1). Hence, reducing the load limiter and deploying air bags early may help reduce chest deflection. Air bag firing time was also found to be an important parameter for BrIC for both models (Fig. 7), showing positive correlation (Appendix I, Fig. I1) and demonstrating that early air bag deployment may help reduce BrIC as well. Other restraint system features that could improve thoracic and head injury response, such as frontal air bag shape, depth, venting and multi-stage inflation, were not considered in this study, nor were multi-stage seat belt load limiters, dual pretensioning or other features, such as seat cushion or knee bolster air bags.

Optimisation results (Table III, Fig. 9) showed that while it was possible to find a single set of restraint parameters that reduced chest deflections, BrIC below the IARV for the F50 model and only BrIC below the IARV for the F50-S model at NCAP Delta-V of 35 mph for a range of PDOFs (0^o, 20^o, 340^o), it was not possible to reduce the chest deflection for the F50-S model below the IARV of 52 mm at Delta-V of 35 mph for PDOF of 0^o and 340^o. Even for PDOF of 20^o, the chest deflection for the F50-S model was very close to the IARV of 52 mm (Fig. 9). To reduce chest deflection for the F50-S model below the IARV of 52 mm, both the load limiter and Delta-V had to be controlled (Table IV, Fig. 10). Analysis of the two mid-sized female models showed the same top five parameters affecting chest deflection, namely Delta-V, PDOF, load limiter, frontal air bag firing time, and knee-to-dash distance (Fig. 7). However, Delta-V was dominant for the F50-S model followed by the load limiter, whereas both load limiter and Delta-V were equally dominant for the F50 model. This may be the reason that chest deflection for the F50 model could be reduced below the IARV by tuning the load limiter, but additional safety measures may be required for the F50-S model. This study shows how differences between two mid-sized female models could affect possible countermeasure designs. Again, this is based on using the small female IARVs for mid-sized females. Further research is needed to help establish these IARVs for mid-sized females.

XGBoost-based ML models were developed using only 149 data points for each human model, which is a relatively small sample size. However, XGBoost models showed the best generalisation (validation scores) compared to all other methods used in this study (Appendix H, Table H1). The trained XGBoost models for both the F50 and F50-S also demonstrated good performance when evaluated on the test dataset, achieving scores above 0.75 (Appendix H, Table H1). XGBoost models were also evaluated to ensure they learned the correct trends (e.g. XGBoost models correctly captured the negative correlation of PDOF with chest deflection and positive correlation of PDOF with BrIC). Since PDOF was converted to a continuous scale, these correlations may not be apparent from the violin plots (Appendix I, Fig. I1) but are clearly discernable in the prediction plots (Figs 8–11). Despite the small sample size, the XGBoost models demonstrated their effectiveness in this study. Increasing the dataset size may help further improve the accuracy of these ML models.

The trained XGBoost models were interpreted using the SHAP Python library to understand the impact of input variables on the output. Other commonly used method for sensitivity analysis is the Sobol method [48]. While SHAP is a model-agnostic method based on the concept of Shapley values, a cooperative game theory concept, the Sobol method is a variance-based global sensitivity approach. The Sobol method focuses on a global measure of a feature's importance, whereas SHAP utilizes Shapley values to provide local explanations of each prediction which are subsequently combined to derive global feature importance. While SHAP has been demonstrated to be a powerful and effective tool for interpreting machine learning models, it also has some limitations. SHAP can be computationally expensive, especially when applied to complex models or large datasets. Additionally, SHAP assumes that the model is additive, meaning that the contribution of each feature is independent of other features. Thus, SHAP may not be able to account for interactions between features.

In this study, results based on 149 paired simulations are presented. These simulations are biased towards lower Delta-Vs (25–30 mph) and higher PDOFs (Appendix G, Fig. G1). In comparison, the majority of real-world

frontal impact crashes are under Delta-V of 25 mph and between PDOF of ±10° [32]. Furthermore, only one vehicle model, specifically the driver compartment extracted from 2014 Honda Accord FE model, was utilised to represent a virtual vehicle population. Additionally, only the crash pulse magnitude was varied, while the shape of the crash pulse remained fixed. The crash pulse shape used in this study does not represent all real-world crashes, and the injury metrics may be influenced by the crash pulse shape. Therefore, the injury metrics and corresponding injury risks computed in this study may not accurately represent similar real-world crashes. Nonetheless, despite not fully representing the field environment, this study does provide important insights into injury risks for mid-sized females.

The combinations of restraint parameters used in this study do not necessarily represent actual real-world representative combinations of restraint system variables. Rather, a wide mix of variables were used, including some that may never be used in an actual vehicle design, such as low belt loads with low air bag mass flow and a later air bag firing time. Consequently, many of the resulting pairs of simulations are for suboptimal designs that result in risk values far higher than an actual optimised set of parameters. However, this wide mix of variables does allow for exploration of the design space, helping to identify sensitivities and potential countermeasures.

This study shows how variability between two mid-sized female models could affect injury risk and the potential countermeasures. This type of information could be useful when developing and selecting HBMs for use in virtual testing.

Although injury risks were evaluated for different body regions, ML-based analysis was only carried out for the brain and thorax body regions as these showed statistically significant differences between the two models, along with high relative risk compared to other body regions. Evaluating other body regions will be part of future work.

Only NASS-CDS data was analyzed in this study. Since 2016, NHTSA has been conducting detailed crash investigations through the Crash Investigation Sampling System (CISS). Analyzing CISS data will be part of future work.

V. CONCLUSIONS

The F50 model showed higher brain injury risk and lower thoracic injury risk compared to the F50-S model. For the F50 model, it was possible to reduce the chest deflection below an exemplar IARV for a range of PDOFs by tuning the load limiter, but for the F50-S model additional safety measures may be required. This study demonstrates how variability between two mid-sized females could affect the injury outcome and the potential countermeasures.

VI. REFERENCES

[1] Klinich, K. D., Bowman, P., Flannagan, C., Rupp, J. D. (2016) Injury patterns in motor-vehicle crashes in the United States: 1998-2014. Technical Report, Report No. UMTRI-2016-16.

[2] Qin, X., Wang, K., Cutler, C. E. (2013) Analysis of crash severity based on vehicle damage and occupant injuries, *Transportation Research Record Journal of the Transportation Research Board*, 2386: 95–102.

[3] Frampton, R., Sferco, R., Welsh, R., Kirk, A., Fay, P. (2000) Effectiveness of airbag restraints in frontal crashes – what European field studies tell us. *Proceedings of IRCOBI Conference*, Montpellier, France.

[4] MacLennan, P. A., McGwin, G., Metzger, J., Moran, S. G., Rue, L. W. (2004) Risk of injury for occupants of motor vehicle collisions from unbelted occupants. *Injury Prevention*, **10**: pp.363–367.

[5] Kahane, C. J. (2013) Effectiveness of pretensioners and load limiters for enhancing fatality reduction by seat belts. Report No. DOT HS 811 835, National Highway Traffic Safety Administration.

[6] Spencer, M. R., Hedegaard, H., Garnett, M. (2021) Motor Vehicle Traffic Death Rates, by Sex, Age Group, and Road User Type: United States, 1999-2019. *National Center for Health Statistics Data Brief*.

[7] Forman, J., Poplin, G. S. *et al.* (2019) Automobile injury trends in the contemporary fleet: Belted occupants in frontal collisions. *Traffic Injury Prevention*, **20**(6): pp.607-612.

[8] Brumbelow, M. L., Jermakian, J. S. (2022) Injury risks and crashworthiness benefits for females and males: which differences are physiological? *Traffic Injury Prevention*, **23**: pp.11–16.

[9] Centers for Disease Control and Prevention (CDC). National Center for Health Statistics (NCHS). National Health and Nutrition Examination Survey Data. Hyattsville, MD: U.S. Department of Health and Human Services, Centers for Disease Control and Prevention, 2015-2016, https://www.cdc.gov/nchs/nhanes/.

[10] Holcombe, S. A., Wang, S. C., Grotberg, J. B. (2017) The effect of age and demographics on rib shape. *Journal of Anatomy*, **231**(2): pp.229–247.
[11] Shi, X., *et al.* (2014) A statistical human rib cage geometry model accounting for variations by age, sex, stature and body mass index. *Journal of Biomechanics*, **47**(10): pp.2277–85.
[12] Weaver, A. A., Schoell, S. L., Stitzel, J. D. (2014) Morphometric analysis of variation in the ribs with age and sex. *Journal of Anatomy*, **225**(2): pp.246–61.
[13] Hwang, E., Hallman, J., *et al*. (2016) Rapid Development of Diverse Human Body Models for Crash Simulations Through Mesh Morphing. SAE Technical Paper 2016-01-1491.
[14] Carlsson, A., Chang, F., *et al.* (2012) EvaRID - A 50th Percentile Female Rear Impact Finite Element Dummy Model. *Proceedings of IRCOBI Conference*.
[15] Sato, F., *et al.* (2017) Effects of Whole Spine Alignment Patterns on Neck Responses in Rear End Impact. *Traffic Injury Prevention*, **18**(2): pp.199–206.
[16] Global Human Body Modeling Consortium (GHBMC), F50-OS, v2.3.1, 2022.
[17] Robinson, A., Kleeck, W. V., Gayzik, S. F. (2023) Development and Preliminary Validation of Computationally Efficient and Detailed 50th Percentile Female Human Body Models. *The Association for the Advancement of Automotive Medicine*, In review.
[18]Global Human Body Modeling Consortium (GHBMC), F05-OS, v2.2, 2019.
[19] Davis, M. L., Koya, B., Schap, J. M., Gayzik, F. S. (2016) Development and Full Body Validation of a 5th Percentile Female Finite Element Model. *Stapp Car Crash Journal*, **60**: pp.509–544.
[20] Gordon, C. C., Churchill, T., *et al.* (1989) 1988 Anthropometric Survey of U.S. Army Personnel: Methods and Summary Statistics. Report No. NATICK/TR-89/044.
[21] McDowell, M. A., Fryar, C. D., Ogden, C. L. (2009) Anthropometric reference data for children and adults: United States, 1988–1994. *National Center for Health Statistics*, **11**(249).
[22] Government Accountability Office. (2023) DOT Should Take Additional Actions to Improve the Information Obtained from Crash Test Dummies. GAO Publication No. 23-105595, Washington, D.C.: U.S. Government Printing Office.
[23] Gordon, C. C., *et al*. (2014) 2012 Anthropometric Survey of U.S. Army Personnel: Methods and Summary Statistics. Report No. NATICK/TR-15/007.
[24] Singh, H., Ganesan, V., *et al*. (2018) Vehicle interior and restraints modeling development of full vehicle finite element model including vehicle interior and occupant restraints systems for occupant safety analysis using THOR dummies. National Highway Traffic Safety Administration, Report No. DOT HS 812 545.
[25] Global Human Body Modeling Consortium (GHBMC), M50-OS, v2.2, 2019.
[26] Schwartz, D., Guleyupoglu, B., *et al.* (2015) Development of a Computationally Efficient Full Human Body Finite Element Model. *Traffic Injury Prevention*, **16**(Suppl 1): S49–S56.
[27] Eppinger, R., Sun, E *et al.* (1999) Development of improved injury criteria for the assessment of advanced automotive restraints systems – II. National Highway Traffic Safety Administration.
[28] Kuppa, S., Wang, J., Haffner, M., Eppinger, R. (2001) Lower extremity injuries and associated injury criteria. *ESV conference*, Paper No. 457.
[29] Takhounts, E. G., Craig, M. J., Moorhouse, K., McFadden, J., Hasija, V. (2013) Development of Brain Injury Criteria (BrIC). *Stapp Car Crash Journal*, **57**: pp.243–266.
[30] Craig, M. J., Parent, D., *et al*. (2020) Injury criteria for THOR 50th male ATD, National Highway Traffic Safety Administration.
[31] Livermore Software Technology Corp. LS-OPT, v5.2.1 (revision 106944).
[32] Takhounts, E. G., Hasija, V., Craig, M. J. (2019) BrIC and field injury risk. *ESV conference*, paper no. 19-0154.
[33] Altman, N., Krzywinski, M. (2015) Simple linear regression. *Nature Methods*, **12**(11): pp.999–1000.
[34] Tibshirani, R. (1996) Regression Shrinkage and Selection via the lasso. *Journal of the Royal Statistical Society*, **58**(1): pp.267–88.
[35] Hoerl, A. E., Kennard, R. W. (1970) Ridge Regression: Biased Estimation for Nonorthogonal Problems. *Technometrics*, **12**(1): pp. 55–67.
[36] Cortes, C., Vapnik, V. N. (1995) Support-vector networks. *Machine Learning*, **20**(3): pp.273–297.
[37] Breiman, L. (2001) Random Forests. *Machine Learning*, **45**(1): pp.5–32.
[38] Chen, T., Guestrin, C. (2016) XGBoost: A Scalable Tree Boosting System. *In Proceedings of the 22nd ACM SIGKDD International Conference on Knowledge Discovery and Data Mining.*
[39] Hastie, T., Tibshirani, R., Friedman, J. (2017) The Elements of Statistical Learning, pp.241–248, *Springer*, NY, USA.

[40] Pedregosa, F., *et al.* (2011) Scikit-learn: Machine Learning in Python. *Journal of Machine Learning Research*, **12**: pp.2825–2830.
[41] Shapley, L. S. (1951) Notes on the n-Person Game -- II: The Value of an n-Person Game. RAND Corporation.
[42] Lundberg, S. M., Lee, S. (2017) A Unified Approach to Interpreting Model Predictions, *Advances in Neural Information Processing Systems*.
[43] Scikit-optimize, v0.8.1, 2020.
[44] Kemper, A. R., *et al*. (2007) The biomechanics of human ribs: material and structural properties from dynamic tension and bending tests. *Stapp Car Crash Journal*, **51**: pp.235–273.
[45] Iwamoto, M., *et al.* (2007) Development of Advance Human Models in THUMS. *Proceedings of 6th European LS-DYNA Users Conference*, pp.47–56.
[46] Total Human Model for Safety (THUMS), AF50 (Whiplash), V4.0.
[47] Osth, J., Mendoza-Vasquez, M., Linder, A., Svensson, M.Y., Brolin, K. (2017) The VIVA OpenHBM Finite Element 50th Percentile Female Occupant Model: Whole Body Model Development and Kinematic Validation, *Proceedings of IRCOBI Conference*, Antwerp, Belgium
[48] Sobol, I. (1993) Sensitivity analysis for non-linear mathematical models. Mathematical Modeling & Computational Experiment, **1**: pp 407–414.

VII. DISCLAIMER

This paper is published in the interest of advancing motor vehicle safety research. The United States Government assumes no liability for its contents or use thereof. If trade or manufacturers' names are mentioned, it is only because they are considered essential to the object of the publication and should not be construed as an endorsement. The United States Government does not endorse products or manufacturers.

VIII. APPENDIX A: MID-SIZED FEMALE ANTHROPOMETRIC MEASUREMENTS AND HUMAN BODY MODEL DETAILS

TABLE A1
MID-SIZED FEMALE ANTHROPOMETRIC MEASUREMENTS AND HBM DETAILS

	F50	F50-S	ANSUR-II (50th Female)	THUMS (50th Female)	VIVA (50th Female)
Number of elements	373,276	374,333	N/A	2311533	769,101
Total mass (kg)	62.04	68.91	66.80	62.00	61.87
Head mass (kg)	3.75	4.01	N/A	3.83	3.74
Head moment of inertia, Ixx (kg.mm^2)	1.30E+04	1.45E+04	N/A	1.31E+04	1.43E+04
Head moment of inertia, Iyy (kg.mm^2)	1.63E+04	1.74E+04	N/A	1.64E+04	1.78E+04
Head moment of inertia, Izz (kg.mm^2)	1.11E+04	1.34E+04	N/A	1.36E+04	1.37E+04
Torso mass (including neck) (kg)	19.20	20.43	N/A	22.45	21.17
Seated height (mm)	848.00	856.00	857.00	843.74	836.62
Chest depth @ 4th rib (mm)*	210.70	256.10	245.00**	200.24	232.93
Chest breadth @ 4th rib (mm)*	348.20	327.70	268.00***	313.15	320.22
Chest depth @ 8th rib (mm)*	204.60	219.70	N/A	191.88	214.92
Chest breadth @ 8th rib (mm)*	306.60	284.10	N/A	302.88	271.50
Shoulder breadth (biacromial) (mm)	375.90	353.50	365.00	339.87	334.30
Femur length (mm)	370.00	393.00	379.00	362.00	360.00
Tibia height (mm)	374.90	365.90	374.00	338.12	355.63
Waist breadth (mm)	283.80	296.40	298.00	293.40	302.14
Waist depth (mm)	222.10	209.20	209.00	199.63	238.16
Hip breadth (mm)	363.80	358.80	353.00	377.86	386.00
Hip depth (mm)	228.10	213.20	N/A	188.00	250.38

** Includes flesh and skin, ** At the most anterior right point on the chest, *** At the level of the most anterior right point on the chest*

IX. APPENDIX B: OCCUPANT POSITIONING

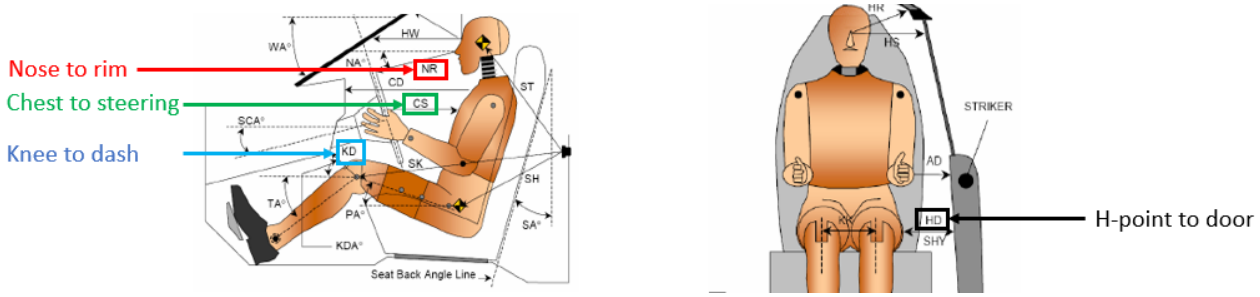

Fig. B1. Test clearance measurements used for positioning the M50 model.

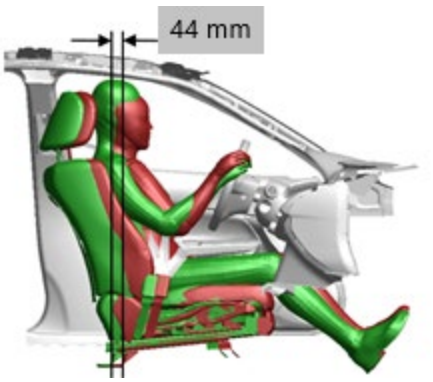

Fig. B2. F50-S (red) and M50 (green) models in baseline seating position.

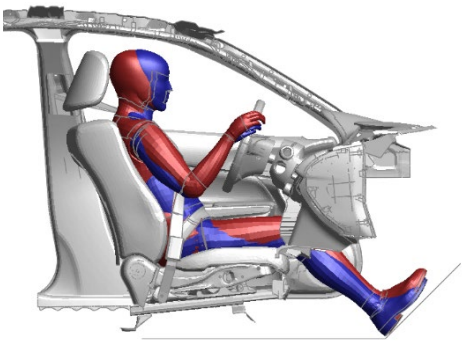

Fig. B3. F50-S (red) and F50 (blue) models in baseline seating position.

X. APPENDIX C: CRASH PULSE

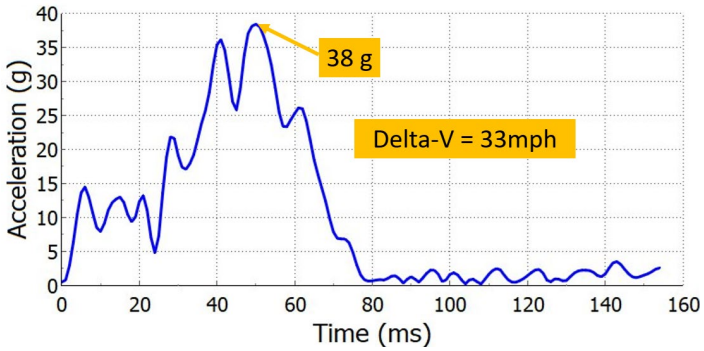

Fig. C1. Baseline crash pulse.

XI. APPENDIX D: CRITICAL INTERCEPTS

TABLE D1
CRITICAL INTERCEPTS

	50th (mid-sized) male	5th (small) female (used for F50 & F50-S)
Tension (N)	3000	2250
Compression (N)	3230	2422
Flexion (Nm)	54.5	27.25
Extension (Nm)	72.0	36.0

XII. APPENDIX E: CRASH AND RESTRAINT PARAMETERS VARIED IN THIS STUDY

TABLE E1
CRASH AND RESTRAINT PARAMETERS

Parameter (*Corresponding name used in figures*)	Baseline value	Minimum value	Maximum value
Crash Parameters			
Delta-V *(DeltaV)*	33 mph	25 mph	45 mph
PDOF *(pdof)*	0°	-30°, -25°, -20°, -15°, -10°, -5°, 0°, 5°, 10°, 15°, 20°, 25°, 30°	
Restraint related Parameters			
Scaling factor for frontal air bag mass flow rate *(FT_airbag_MassFlow)*	1.0	0.75	1.25
Scaling factor for side curtain air bag mass flow rate *(Side_airbag_MassFlow)*	1.0	0.75	1.25
Frontal and side curtain air bag firing time *(FT_airbag_FiringTime)*	14 ms	5 ms	45 ms
Collapsible column force *(Collapsible_Column_Stiffness)*	3000 N	3000 N	12000 N
Load limiter *(Load_Limiter_MaxLoad)*	3000 N	1000 N	5000 N
Pretensioner *(Pretensioner_LimitingForce)*	1000 N	1000 N	3000 N
Side curtain air bag – head friction coefficient *(Head_to_Side_Airbag_Friction)*	0.3	0.001	1.0
Frontal air bag – head friction coefficient *(Head_to_FT_Airbag_Friction)*	0.3	0.001	1.0
Floor-shoe friction coefficient *(Friction_ShoeFloor)*	0.5	0.001	0.5
Knee-to-dash distance *(Dash_to_Knee_50th)*	1.0	0.75	1.25

XIII. APPENDIX F: RESTRAINT PARAMETERS VARIED FOR OPTIMISATION

TABLE F1

PARAMETERS VARIED FOR OPTIMISATION

Restraint parameter	Range
Frontal air bag mass flow rate	0.75–1.25
Steering column collapse force	3000 N–12000 N
Load limiter	1200 N–5000 N
Pretensioner	1000 N–3000 N
Frontal and side curtain air bag firing time	5 ms–45 ms
Side curtain air bag mass flow rate	0.75–1.25
Head-frontal air bag friction coefficient	0.001–1.0
Head-side curtain air bag friction coefficient	0.001–1.0

XIV. APPENDIX G: DELTA-V AND PDOF DISTRIBUTION FOR 149 PAIRED SIMULATIONS

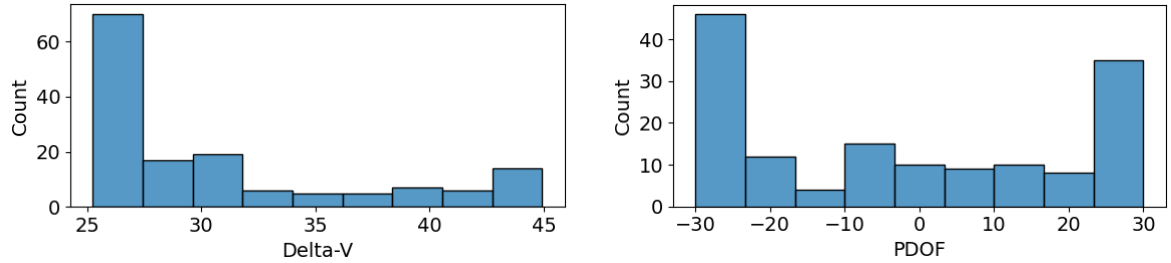

Fig. G1. Delta-V and PDOF distribution.

XV. APPENDIX H: CORRELATION COEFFICIENT FOR ML MODELS

TABLE H1

CORRELATION COEFFICIENT (R)

F50						
ML Models	BrIC			Chest deflection		
	Training	Validation	Test	Training	Validation	Test
Linear Regression	0.61	0.42	X	0.81	0.71	X
Ridge (L2)	0.61	0.42	X	0.81	0.72	X
Lasso (L1)	0.60	0.44	X	0.81	0.71	X
SVR	0.81	0.45	X	0.78	0.67	X
Random Forest	0.92	0.68	X	0.97	0.83	X
XGBoost	0.99	**0.78**	**0.85**	0.99	**0.92**	**0.91**
F50-S						
ML Models	BrIC			Chest deflection		
	Training	Validation	Test	Training	Validation	Test
Linear Regression	0.58	0.42	X	0.83	0.77	X
Ridge (L2)	0.58	0.43	X	0.83	0.78	X
Lasso (L1)	0.57	0.42	X	0.83	0.78	X
SVR	0.71	0.48	X	0.85	0.76	X
Random Forest	0.90	0.64	X	0.97	0.78	X
XGBoost	0.99	**0.77**	**0.76**	0.99	**0.87**	**0.89**

XVI. APPENDIX I: VIOLIN PLOTS SHOWING CORRELATION

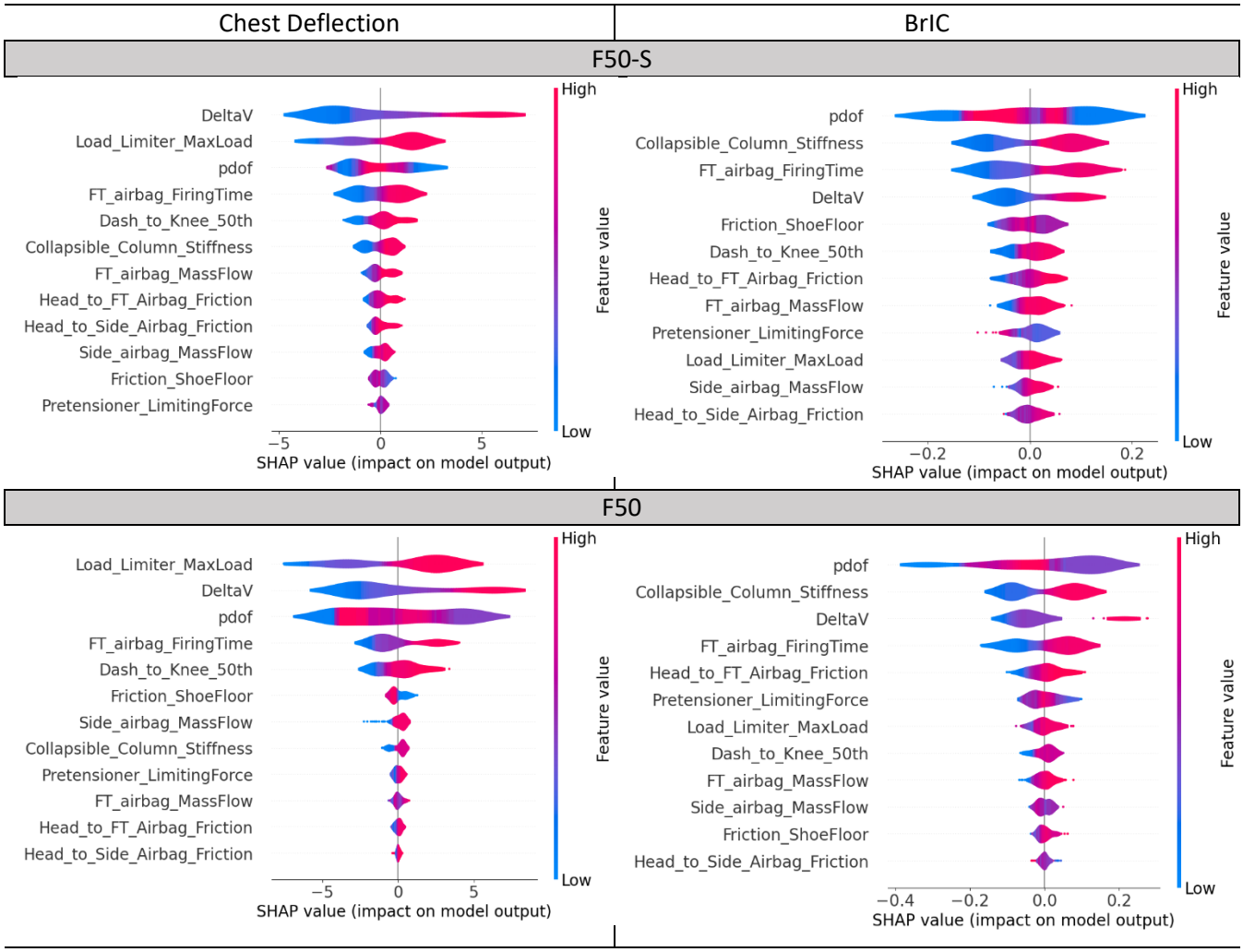

Fig. I1. Violin plots for chest deflection and BrIC for the F50-S and F50 models.